scientific reports

Check for updates

OPEN

Reduced-order linearized dynamic model for induction motor-driven centrifugal fan-pump system

Cebrail Turkeri[1], Oleh Kiselychnyk[2], Serdar Ekinci[3], Davut Izci[4,5], Mohit Bajaj[6,7,9]✉ & Oleksandr Rubanenko[8]✉

The inherent complexity and nonlinear nature of the dynamic representation of an induction motor-operated centrifugal fan/pump (CFP) system hinders the systematic closed-loop control design for flow rate (Q) and pressure/head (H) regulation, widely used electrical energy-efficient solution in fluid transport infrastructures and designed intuitively nowadays by practical electrical engineers under the implementation constraints of industrial AC drives. This paper derives the system model allowing direct application of analytical closed-loop control design methodologies, avoiding heuristic solutions and it succeeds in the linearization of an experimentally validated nonlinear six-order dynamic representation of the fan coupled with a scalar-controlled induction machine for an arbitrary operating point. It also reduces the model order via derivations in the stator voltage vector reference frame. The results are verified via simulations and experiments. The analytically derived control-oriented linearized model is of third order and relates small deviations of the stator voltage frequency to the corresponding small deviations of the Q and H, suitable for scalar induction motor regulation applications. The model is presented as block diagrams, in state-space representation and computed as transfer functions. Simulated step responses of the linearized and nonlinear models are close and in good agreement with experimental data. Overall, this paper, for the first time, linearizes and reduces the order of the experimentally validated nonlinear model of the fan-induction motor system accounting for the fan's own dynamics. The obtained model is suitable for analytical closed-loop control design by practical electrical engineers, with following implementation based on industrial AC drives.

Keywords Reduced-order method, Centrifugal fans/pumps, Induction motor drives applications, Linearization

Centrifugal fan/pump (CFP) units are commonly utilized in both air distribution and water delivery infrastructures. These systems typically rely on squirrel-cage induction motors due to their cost-effectiveness and operational reliability[1]. In industrialized countries, approximately 60% of the total electromechanical energy conversion done by induction motor drives is for air and water transportation[2]. Due to continuous operation and the input power required for the fans/pumps (FPs) for air distribution and water pumping is proportional to the cube of their speed, there is a huge potential for energy saving[3]. Application of adjustable speed motor drives for FPs flow rate (Q) or pressure (head) (H) control leads up to 30% of electrical energy saving compared to valve regulation[4,5]. Further improvement is achieved via implementation of closed-loop control[6,7], allowing accurately to satisfy demands in air and water and to reduce wasting of electricity and water. It happens owing to automatic adjustment of the FPs velocity reference as the output of the Q or H controller. The velocity reference can also be updated based on the estimated demand algorithms[3]. The required controllers, usually proportional-integral (PI) or proportional-integral-derivative (PID), and their parameters are chosen heuristically[6,7] due to a lack of control-oriented models admitted for practical applications.

[1]Department of Computer Engineering, Batman University, Batman 72100, Turkey. [2]School of Engineering, University of Warwick, Coventry, UK. [3]Department of Computer Engineering, Bitlis Eren University, Bitlis 13100, Turkey. [4]Department of Electrical and Electronic Engineering, Bursa Uludag University, Bursa 16059, Turkey. [5]Applied Science Research Center, Applied Science Private University, Amman 11931, Jordan. [6]Department of Electrical Engineering, Graphic Era (Deemed to Be University), Dehradun 248002, India. [7] Hourani Center for Applied Scientific Research, Al-Ahliyya Amman University, Amman, Jordan. [8]Department of Power Plants and System, Vinnytsia National Technical University, Vinnytsia 21000, Ukraine. [9]Graphic Era Hill University, Dehradun 248002, India. ✉email: mohitbajaj.ee@geu.ac.in; rubanenko.o.y@vntu.edu.ua

Designing control for air and water supply systems requires, from electrical and automation engineers and researchers, some knowledge both on electrical drives and CFPs. The models suitable for accurate simulations[8] consist of two parts: the model of the squirrel-cage induction motor and the FP model itself, interconnected through the shaft angular velocity and the load torque imposed by the FP on the motor shaft. Note that since the principle of operation of centrifugal fans and pumps is the same then their modelling is almost identical except accounting for the static head for pumps.

Induction motor modelling for fans and pumps

The dynamical two-phase modelling of three-phase induction motors is well-established and widely used for design of variable frequency drives. For CFP applications, mainly open velocity loop scalar control is used setting specific relationship between the amplitude and frequency of the voltages supplied to the stator. V/f = constant or V/f^2 = constant laws are available in industrial AC drives[9,10]. More sophisticated adaptive version is suggested in[11], which facilitates raising the initial torque output up to its nominal level. Modelling is carried out in the stator reference frame, the model is nonlinear of fifth order and its electrical variables are sinusoidal signals[12] which does not allow a straightforward analytical closed-loop control design. It can be overcome by applying a vector control also available in the industrial AC drives, but it makes the system unnecessarily more complicated[2,13]. Frequently the impact of the FPs upon AC machines is modelled as a static parabolic dependence of the motor load torque on its velocity[2,14,15]. In all cases this oversimplification[16] is not suitable for closed loop Q or H control design.

Quasi-steady approach to the modelling of centrifugal fan and pump units in motor drive applications

Quasi-steady CFPs (themselves, without motors) modelling means using only steady-state dependences for their description. Then, the fluid flow Q and generated H of the system vary synchronously with the rotational speed of the driving motor. These relationships define how H, shaft power (P), or efficiency (η) vary as a function of the Q, obtained experimentally for various constant velocities[16–18]. The dependences can also be computed based on a system of theoretical and empirical energy loss equations[19] but a huge number of equations and their geometrical parameters to be determined makes this procedure rather applicable for the CFP design than for the control applications. Similar approach extracting the geometry from the datasheet values yields a 5–20% computational error[20]. Note that the pump curves provided by manufacturers are subject to ISO 9906 standard which defines 3.5% tolerance for Q and H and 4% for the power consumption according to the grade 2 accuracy criteria and the requirements are higher for grade 1 (0.5–10 MW)[21].

The quasi-steady modelling is used for accurate required motor power determination[4], and for selection of the best efficient operating point and justifying energy saving control algorithms[6,7]. In[22] a variation of the pump's quasi-steady model with assumed constant efficiency was integrated with an intuitive first-order differential equation (DE) approximating induction machine dynamics and ignoring transients in electromagnetic circuits, with following linearization based on the Taylor expansion approach. Excluding the dynamics of a water tank, it is a first-order linear approximation around a nominal point which was not verified in simulations and experiments, and it is difficult for parameterization.

Quasi-steady CFPs modelling also found application in design of their state estimators. The high expense associated with applying closed-loop control may be mitigated through substituting H and Q sensors with estimators that rely on voltage and current measurements already present in the monitoring systems of electrical drives[12,21,23–25]. The main drawback of these techniques lies in the fact that the prediction is obtained through secondary predictions, compromising accuracy. As expected, the quasi-steady estimators lose validity during transient conditions and the control must be designed sufficiently slow to be considered as quasi-steady[12,26]. Since the quasi-steady models ignore the CFP own dynamics, they should be avoided for analytical closed-loop control design.

Dynamical fan/pump modelling for control applications

The studies in[12] and[13] introduced intuitive dynamic extension to the conventional quasi-steady models. They incorporate a first-order nonlinear DE to represent transient behavior of the Q and are subsequently reorganized into a structure appropriate for control purposes. In[12], the model is coupled with a two-phase representation of the induction motor, allowing the design of the motor velocity and torque estimators, followed by the design of quasi-steady enhanced Q and H estimators. In[13], the model is extended by common motor and pump faults descriptions, enabling analytical design of a fault detection algorithm based on head and electrical measurements. Both studies assume a constant pump efficiency, which limits their applicability to a narrow pump operating range. Further improvements overcome this problem via adding an overall efficiency estimator into the model based on the experimental or datasheet Q–η curves[27] or adding the motor consumed power estimator for following load torque computations[28]. The dynamical models above were not directly validated via experiments. Indirect validation is presented in[26] where the dynamical Q and H estimators accounting for the centrifugal fan dynamics resolve the problem of the quasi-steady estimation failure during transients.

The most recent advances of the FPs dynamical modelling are presented in paper[8]. This includes a new approximation of the Q–H curve at rated velocity allowing modelling of the FPs with a maximum point in the curve. The motor load torque in the model is determined from the FPs' efficiency extracted from the total efficiency estimated by neural network, correctly reflecting the power balance and thus improving accuracy. For the first time, the necessity of the DE for the Q is directly validated experimentally via step responses and it is shown that H can be represented through an algebraic equation. Additionally, indirect model validation is demonstrated through the design and performance comparison of the dynamical and quasi-steady Q and

H neural network estimators. The model is complex and nonlinear, suitable for accurate simulations of the centrifugal FPs in control applications.

Contributions of the paper

This paper for the first time analytically derives and validates the reduced-order linearized dynamic model of the induction motor-driven centrifugal fan-pump system suitable for the analytical closed-loop control design. The linearization is applied to a relatively recently presented nonlinear model[8] which for the first time experimentally justified the necessity to account for the flow rate transients in the fan/pump housing. At present time, flow rate and pressure (head) fan/pump controllers are still chosen intuitively and their parameters are adjusted via iterative simulations and experiments, simulations are done based on quasi-steady models which account for electric motors dynamics only like in[6,7]. The contributions of this work are listed below.

- The linearization is performed around an arbitrary operating point. Although scalar motor control is assumed, linearization is carried out in a synchronous reference frame defined by the alignment with the stator voltage vector, which reduces the order of the combined FP and motor model from six to three, while still maintaining applicability for scalar control (with the stator voltage frequency as the control input). The parameters of the linearized model are dependent on the steady-state values.
- The obtained linearized model is converted to a single input single output (SISO) format, which is convenient for analytical closed loop Q or H control design. This includes block diagrams, state-space representations, and transfer functions suitable for practical implementation.
- The linearized model is validated via simulation and comparison with the simulation of the nonlinear model[8] and against the experimental step response transients.

Analytical derivations

Nonlinear model of a centrifugal fan driven by a three-phase induction motor

The dynamic behavior of the flow rate Q within the fan housing is represented by the following nonlinear DE[8].

$$\chi \frac{dQ}{dt} = H_{or}\left(\frac{\omega}{\omega_r}\right)^2 - a_f Q^2 - b_f Q - a_n Q^2 \tag{1}$$

In this equation, t denotes time, while ω refers to the angular speed of the motor or fan under the assumption of direct-drive operation (i.e., no gearbox). The symbol ω_r indicates the nominal rotational speed and H_{or} represents the fan pressure at zero flow under rated speed conditions. The constants a_f and b_f are empirical parameters reflecting the flow–head (Q-H) relationship at nominal speed, while a_n corresponds to the coefficient for duct-related Q-H characteristics. The parameter χ is a scalar constant introduced through the integration process. The first term on the right-hand side quantifies H under $Q = 0$ and arbitrary ω, as determined by the affinity law. When modeling a pump instead of a fan, the pressure term is substituted by water head, and a constant static head component is deducted accordingly.

The initial three components on the right-hand side of Eq. (1) collectively represent the total pressure generated by the fan, or the equivalent head in the case of pump operation.

$$H = H_{or}\left(\frac{\omega}{\omega_r}\right)^2 - a_f Q^2 - b_f Q \tag{2}$$

When $\chi = 0$, Eq. (1) defines the steady-state operating condition of the fan or pump. All model parameters other than χ can typically be obtained from manufacturer specifications or derived using steady-state experimental data. However, χ is sensitive to operating conditions and must be experimentally identified through dynamic testing procedures. The fan-induced mechanical torque T_L exerted on the motor shaft is calculated in Eq. (3)[8]:

$$T_L = \frac{QH}{\eta_f \omega} \tag{3}$$

where η_f is the FP's own efficiency. For the pump modelling H is multiplied by the density of the water and the gravitation constant to convert [m] into [Pa]. The FP own efficiency is determined as a ratio of the combined (overall) motor/FP efficiency and the motor efficiency;

$$\eta_f = \frac{\eta_c}{\eta_m} \tag{4}$$

The combined efficiency is determined based on the steady-state experimental data using either a neural network estimator or a look-up table or approximation polynomials;

$$\eta_c = f(Q, H, f) \tag{5}$$

where f denotes the frequency of the motor stator voltages.

The FP is actuated by a three-phase squirrel-cage induction motor, which is represented mathematically as an equivalent two-axis machine using the d-q coordinate system rotating at angular speed ω_e[29].

$$\begin{aligned} v_{sd} &= R_s i_{sd} + \frac{d\Psi_{sd}}{dt} - \omega_e \Psi_{sq} \\ v_{sq} &= R_s i_{sq} + \frac{d\Psi_{sq}}{dt} + \omega_e \Psi_{sd} \\ 0 &= R_r i_{rd} + \frac{d\Psi_{rd}}{dt} - (\omega_e - p_n\omega)\,\Psi_{rq} \\ 0 &= R_r i_{rq} + \frac{d\Psi_{rq}}{dt} + (\omega_e - p_n\omega)\,\Psi_{rd} \\ J\frac{d\omega}{dt} &= T - T_L \end{aligned} \tag{6}$$

In the above equations, v, i, Ψ represent voltage, current, and magnetic flux linkage, respectively. The symbol R corresponds to electrical resistance. The indices s and r are used to indicate stator- and rotor-related quantities, while the subscripts d and q refer to components along the direct and quadrature axes in the rotating reference frame. The parameter p_n denotes the number of pole pairs in the motor. J refers to the total moment of inertia acting on the motor shaft, which comprises both the inertia of the fan or pump and the contribution from the fluid medium (air or water) within the duct or pipeline. The electromagnetic torque generated by the motor is defined as follows.

$$T = \frac{3}{2} p_n \frac{L_m}{L_s} (\Psi_{sq} i_{rd} - \Psi_{sd} i_{rq}) \tag{7}$$

Here, L_m corresponds to the magnetizing inductance and L_s is the stator inductance. The magnetic behavior of the machine is considered linear.

$$\begin{aligned} \Psi_{sd} &= L_s i_{sd} + L_m i_{rd} \\ \Psi_{sq} &= L_s i_{sq} + L_m i_{rq} \\ \Psi_{rd} &= L_m i_{sd} + L_r i_{rd} \\ \Psi_{rq} &= L_m i_{sq} + L_r i_{rq} \end{aligned} \tag{8}$$

where L_r is the rotor inductance. Therefore, the model of the centrifugal FP comprises of the FP model itself (1)-(5) and the standard model of the induction machine (6)-(8). These two models are interconnected through ω and T_L. Although the model (1)-(8) is nonlinear and of sixth order, it can be effectively implemented and simulated within the MATLAB/Simulink/Simscape environment by utilizing the induction motor block (SI units) available in the *Specialized Power Systems Toolbox*. For scalar control strategies, the stator reference frame is selected, whereas vector control schemes require operation in a synchronously rotating coordinate frame. To represent Eqs. (6)–(8) in the α-β stationary reference frame, ω_e is equated to zero and indices d and q are replaced by α and β, respectively. No CFP block is available for dynamical modelling in Simscape (only quasi-steady blocks are available), so it must be modelled based on (1)–(5).

It is worth noting that the control design for the induction machines is well established area providing many explicit analytical solutions. At the same time, heuristic solutions, usually PI or PID-controllers, are applied for the FPs Q and H control with iterative adjustments of parameters via simulations and experiments. Due to the high order, nonlinearity and complexity of the combined model, the analytical closed-loop Q and H control design is quite challenging. The goal of the present paper is to develop and verify experimentally a linearized reduced-order FP model suitable for and facilitating the analytical close-loop control design procedures.

Linearized representation of the centrifugal fan actuated by an induction motor

In equations, the system variables, inputs and disturbances are considered as sums of their steady-state values and corresponding small deviations. The difference of these equations with corresponding steady-state equations and neglecting terms with small values of the second and higher orders yield the linearized description in deviations. Performing the linearization of Eq. (1) about an arbitrary operating point with $Q = Q_s$ and $\omega = \omega_s$, the corresponding parameters to this point are found as $\chi = \chi_s$, $a_f = a_{fs}$, $b_f = b_{fs}$ and $a_n = a_{ns}$. Based on (1) the steady-state equation is written as:

$$\chi_s . \frac{dQ_s}{dt} = 0 = H_{or} . \left(\frac{\omega_s}{\omega_r}\right)^2 - a_{fs} . {Q_s}^2 - b_{fs} . Q_s - a_{ns} . {Q_s}^2 \tag{9}$$

Assuming that the velocity ω_s and parameter a_{ns} obtained small perturbations $\delta\omega$ and δa_n, respectively, the flow rate Q_s and parameters χ_s, a_{fs} and b_{fs} will obtain the corresponding deviations δQ, $\delta\chi$, δa_f and δb_f. Consequently, Eq. (9) can be put into the following view.

$$\begin{aligned} (\chi_s + \delta\chi) \cdot \frac{d\,(Q_s + \delta Q)}{dt} = &- (a_{fs} + a_{ns} + \delta a_f + \delta a_n) \cdot (Q_s + \delta Q)^2 \\ &- (b_{fs} + \delta b_f) \cdot (Q_s + \delta Q) + H_{or} \cdot \left(\frac{\omega_s + \delta\omega}{\omega_r}\right)^2 \end{aligned} \tag{10}$$

Subtracting (9) from (10) and neglecting small values of second order and higher yields the linearized DE for the flow rate (11) whose parameters depend on the steady-state conditions. They are constant around the specific steady state but different for different operating points.

$$\chi_s \cdot \frac{d\delta Q}{dt} = -\left[2Q_s \cdot (a_{fs} + a_{ns}) + b_{fs}\right] \cdot \delta Q + 2\omega_s \cdot \frac{H_{or}}{{\omega_r}^2} \cdot \delta\omega - {Q_s}^2 \cdot (\delta a_f + \delta a_n) - Q_s \cdot \delta b_f \tag{11}$$

By employing the same linearization technique used in Eqs. (2) and (3), one can derive linear algebraic expressions representing the variations in pressure output δH and the torque δT_L generated by the fan or pump on the motor shaft.

$$\delta H = -\left(2a_{fs} \cdot Q_s + b_{fs}\right) \cdot \delta Q + 2\omega_s \cdot \frac{H_{or}}{{\omega_r}^2} \cdot \delta\omega - {Q_s}^2 \cdot \delta a_f - Q_s \cdot \delta b_f \tag{12}$$

$$\delta T_L = \frac{Q_s}{\eta_{fs.}\omega_s} \cdot \delta H + \frac{H_s}{\eta_{fs.}\omega_s} \cdot \delta Q - \frac{T_{Ls}}{\omega_s} \cdot \delta\omega - \frac{T_{Ls}}{\eta_{fs}} \cdot \delta\eta_f \tag{13}$$

Scalar control strategies based on constant voltage-frequency ratio (V/f) or voltage-frequency-squared ratio (V/f^2) ratios are commonly employed in driving induction motors coupled to CFPs. While the implementation of the model is typically carried out within the $\alpha - \beta$ stationary reference frame, analytical simplification and linearization steps are more efficiently conducted within the synchronous reference frame oriented along the stator voltage vector. In this case, $\omega_e = \omega_{0el} = 2\pi f$, $v_{sq} = 0$ and $v_{sd} = |v_s|$. When assuming a negligible stator resistance (i.e., $R_s \approx 0$), the first two expressions in system (6) reduce to a single algebraic equation describing the stator-side dynamics:

$$\begin{aligned} \frac{|v_s|}{\omega_{0el}} &= -\Psi_{sq} = const \\ \Psi_{sd} &= 0 \end{aligned} \tag{14}$$

By incorporating this condition into the Eqs. (3) and (4) of system (6), along with the relationship presented in Eq. (8), a refined description of the rotor-side circuit behavior can be obtained.

$$\begin{aligned} 0 &= R_r i_{rd} + \frac{L_r}{L_s}\sigma\frac{di_{rd}}{dt} - s\omega_{0el}\frac{L_m}{L_s}\Psi_{sq} - s\omega_{0el}\frac{L_r}{L_s}\sigma i_{rq} \\ 0 &= R_r i_{rq} + \frac{L_r}{L_s}\sigma\frac{di_{rq}}{dt} + s\omega_{0el}\frac{L_r}{L_s}\sigma i_{rd} \end{aligned} \tag{15}$$

In the equation above, the slip is s and the symbol $\sigma = \left(L_s L_r - L_m^2\right)/L_r$. Equation (15) is inherently nonlinear due to the multiplicative interaction of several variables including ω_{0el}, s, i_{rd} and i_{rq}. Ψ_{sq} is treated as a constant and is no longer considered a variable. Applying a linearization process similar to that used in Eq. (1), the deviation-based formulation of the rotor circuit dynamics is obtained as follows.

$$\begin{aligned} T_{es}\frac{d\delta i_{rd}}{dt} + \delta i_{rd} &= \frac{s_s}{s_{crs}}\delta i_{rq} + \left(\frac{i_{rqs}}{s_{crs}} + \frac{L_m}{L_s}\frac{\omega_{0els}\Psi_{sq}}{R_r}\right)\delta s \\ T_{es}\frac{d\delta i_{rq}}{dt} + \delta i_{rq} &= -\frac{s_s}{s_{crs}}\delta i_{rd} - \frac{i_{rds}}{s_{crs}}\delta s \end{aligned} \tag{16}$$

Here, $s_{crs} = \frac{L_s R_r}{L_r \sigma \omega_{0els}}$ denotes the critical slip associated with a given electrical angular frequency. The parameter $T_{es} = \frac{L_r}{L_s}\sigma\frac{1}{R_r} = \frac{1}{s_{crs}\omega_{0els}}$ represents the electrical time constant and subscript 's' indicates steady-state values. Using Eqs. (7) and (14), the torque deviation for the motor can be formulated as in (17).

$$\delta T = \frac{3}{2}p_n\frac{L_m}{L_s}\Psi_{sq}\delta i_{rd}. \tag{17}$$

By combining Eqs. (16) and (17), and incorporating Eqs. (14) and (15), a linearized differential expression governing the torque deviation is derived.

$$T_{es}\frac{d\delta T}{dt} + \delta T = \frac{3}{2}p_n\left(\frac{L_m}{L_s}\right)^2\frac{|v_s|_s^2}{R_r\omega_{0els}}\delta s. \tag{18}$$

With $s = \left(\omega_{0el} - p_n\omega\right)/\omega_{0el}$, the linearization yields the following for the slip deviation.

$$\delta s = \left(\delta\omega_0 - \delta\omega\right)/\omega_{0s} \tag{19}$$

Here, $\omega_{0s} = 2\pi f_s/p_n = \omega_{0els}/p_n$ represents the motor's no-load angular velocity corresponding to a given supply frequency. Substituting Eq. (19) into (18) yields:

$$T_{es}\frac{d\delta T}{dt}+\delta T=\beta_s\delta\omega_0-\beta_s\delta\omega=\frac{2\pi}{p_n}\beta_s\delta f-\beta_s\delta\omega \tag{20}$$

where $\beta_s=\frac{3}{2}p_n\left(\frac{L_m}{L_s}\right)^2\frac{|v_s|_s^2}{R_r\omega_{0els}\omega_{0s}}$.

If R_s cannot be neglected, then the reference frame can be aligned with the vector of the stator voltage excluding the drop of the voltage across the stator resistance. Keeping the ratio of this vector magnitude and the voltage frequency constant instead of the V/f = const regulation is equivalent to neglecting the stator resistance and modelling leads to the same Eq. (20) where β_s is computed based on this vector magnitude instead of the stator voltage magnitude.

The final equation from system (6), reformulated in terms of deviations, is expressed as:

$$J_s\frac{d\delta\omega}{dt}=\delta T-\delta T_L \tag{21}$$

The linearized dynamic representation of the squirrel-cage induction motor, described by Eqs. (20) and (21), constitutes a second-order system. This formulation corresponds to a constant voltage-to-frequency (V/f) control strategy under the assumption of negligible stator resistance. Although initially formulated in a synchronous reference frame oriented along the stator voltage vector, the model retains its applicability in the stationary frame due to the control input being represented by the frequency deviation δf. Moreover, the same framework can be extended to V/f^2-based control schemes, provided that the voltage–frequency relationship is approximated as piecewise linear.

Additionally, the linearized model of the coupled FP system powered by the induction machine, represented by Eqs. (11), (20), and (21), is of third order and incorporates two additional algebraic relations, namely Eqs. (12) and (13). The parameters of the model depend on the operating conditions, and it should be accounted for in case of the model application for control design. For a specific narrow control range, the linearized model demonstrates superior accuracy over the nonlinear alternative due to higher accuracy of the approximation parameters. Further conversion of the model depends on what is required to be controlled and expected analytic control design procedure.

Linearized representation of flow rate behaviour

To construct the flow rate model, Eq. (12) is first substituted into (13), followed by inserting the resulting expression into Eq. (21). It allows us to eliminate the algebraic equations and the model includes only three DEs of the first order.

$$\begin{aligned}\chi_s\frac{d\delta Q}{dt}&=-k_{Qs}\delta Q+k_{\omega s}\delta\omega-Q_s^2\left(\delta a_f+\delta a_n\right)-Q_s\delta b_f\\ J_s\frac{d\delta\omega}{dt}&=\delta T-k_{TQs}\delta Q-k_{T\omega Qs}\delta\omega+k_{TafQs}\delta a_f+k_{TbfQs}\delta b_f+k_{T\eta s}\delta\eta_f\\ T_{es}\frac{d\delta T}{dt}&=-\delta T+k_{fs}\delta f-\beta_s\delta\omega\end{aligned} \tag{22}$$

where $k_{Qs}=2Q_s(a_{fs}+a_{ns})+b_{fs}$, $k_{\omega s}=2\omega_s\frac{H_{or}}{\omega_r^2}$, $k_{TQs}=\frac{H_s-\left(2a_{fs}Q_s+b_{fs}\right)Q_s}{\eta_{fs}\omega_s}$,

$k_{T\omega Qs}=2\frac{H_{or}Q_s}{\omega_r^2\eta_{fs}}-\frac{T_{Ls}}{\omega_s}$, $k_{TafQs}=\frac{{Q_s}^3}{\eta_{fs}\omega_s}$, $k_{TbfQs}=\frac{{Q_s}^2}{\eta_{fs}\omega_s}$, $k_{T\eta s}=\frac{T_{Ls}}{\eta_{fs}}$, $k_{fs}=\beta_s\frac{2\pi}{p_n}$.

The block diagram corresponding to system (22) is depicted in Fig. 1. Note that disturbances δa_f, δb_f and $\delta\eta_f$ are considered as independent, although they depend on control action δf, control output δQ and independent disturbance δa_n. For a narrow control range, they can be neglected. 'S' denotes the differentiation operator to distinguish it with the slip 's'.

Linearized model of the pressure dynamics

For the pressure modelling, express δQ from (12) and eliminate δQ from (11) and (13). Then the pressure dynamics model will only consist of three DEs:

$$\begin{aligned}\chi_s\frac{d\delta H}{dt}&=-k_{Hs}\delta H-k_{H\omega s}\delta\omega-k_{Hafs}\delta a_f-k_{Hbfs}\delta b_f-Q_s^2\delta a_n+k_{H\omega ds}\frac{d\delta\omega}{dt}\\ &\quad-k_{Hafds}\frac{d\delta a_f}{dt}-k_{Hbfds}\frac{d\delta b_f}{dt}\\ J_s\frac{d\delta\omega}{dt}&=\delta T-k_{THs}\delta H-k_{T\omega Hs}\delta\omega+k_{TafHs}\delta a_f+k_{TbfHs}\delta b_f+k_{T\eta s}\delta\eta_f\\ T_{es}\frac{d\delta T}{dt}&=-\delta T+k_{fs}\delta f-\beta_s\delta\omega\end{aligned} \tag{23}$$

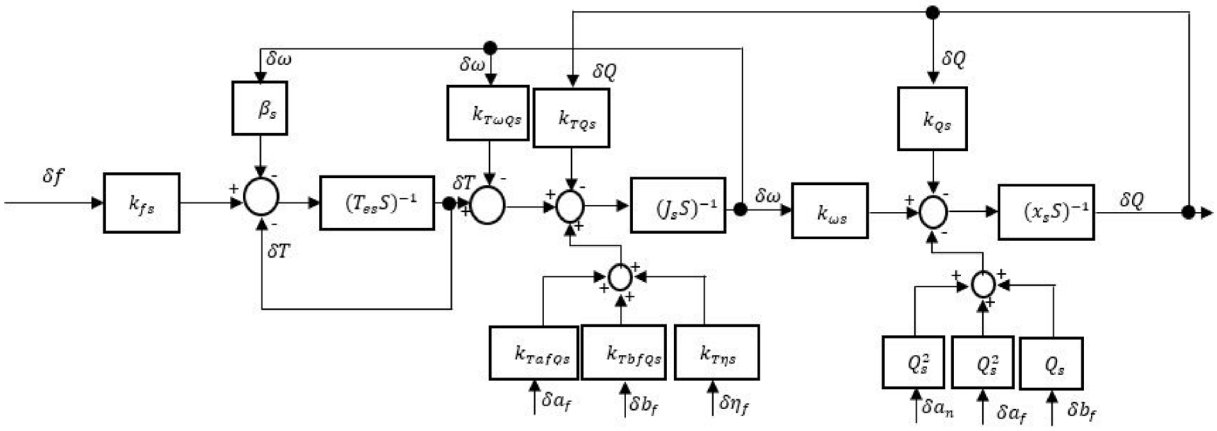


Fig. 1. Block diagram of the model of the fan actuated by an induction motor under flow rate control configuration linearized around an arbitrary operating point.

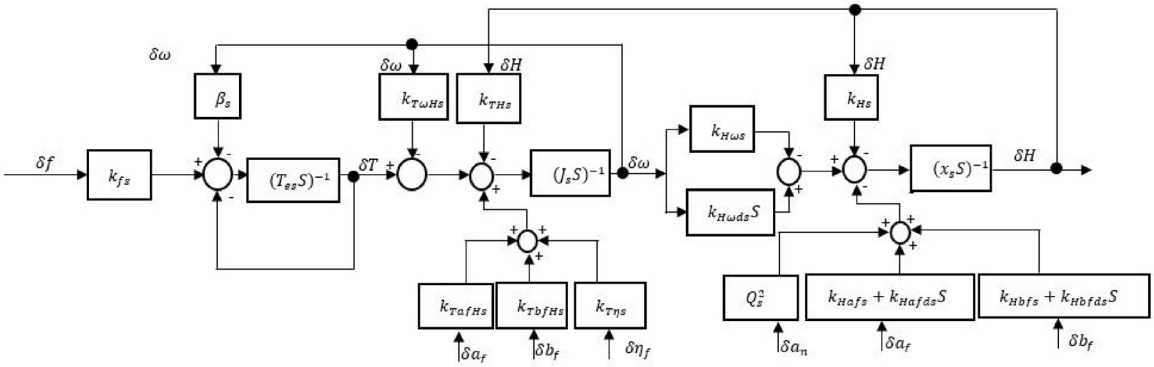


Fig. 2. Block diagram of the model of the fan actuated by an induction motor under pressure control configuration linearized around an arbitrary operating point.

where $k_{Hs} = 2Q_s(a_{fs} + a_{ns}) + b_{fs}$, $k_{H\omega s} = \left[2\omega_s \frac{H_{or}}{\omega_r^2} - \frac{\left(2Q_s\left(a_{fs}+a_{ns}\right)+b_{fs}\right)2\omega_s \frac{H_{or}}{\omega_r^2}}{2a_{fs}Q_s+b_{fs}}\right](2a_{fs}Q_s + b_{fs})$,

$k_{Hafs} = \left[\frac{\left(2Q_s\left(a_{fs}+a_{ns}\right)+b_{fs}\right)Q_s^2}{2a_{fs}Q_s+b_{fs}} - Q_s^2\right](2a_{fs}Q_s + b_{fs})$, $k_{Hbfs} = b_{fs}\left[\frac{\left(2Q_s\left(a_{fs}+a_{ns}\right)+b_{fs}\right)Q_s}{2a_{fs}Q_s+b_{fs}} - Q_s\right](2a_{fs}Q_s + b_{fs})2\omega_s \frac{H_{or}}{\omega_r^2}$

$k_{Hafds} = \chi_s Q_s^2$, $k_{Hbfds} = \chi_s Q_s$, $k_{THs} = \frac{Q_s}{\eta_{fs}\omega_s} - \frac{H_s}{\eta_{fs}\omega_s(2a_{fs}Q_s+b_{fs})}$, $k_{T\omega Hs} = \frac{H_s}{\eta_{fs}\omega_s}\frac{2\omega_s \frac{H_{or}}{\omega_r^2}}{2a_{fs}Q_s+b_{fs}} - \frac{T_{Ls}}{\omega_s}$,

$k_{TafHs} = \frac{H_s}{\eta_{fs}\omega_s}\frac{Q_s^2}{2a_{fs}Q_s+b_{fs}}$, $k_{TbfHs} = \frac{H_s}{\eta_{fs}\omega_s}\frac{Q_s}{2a_{fs}Q_s+b_{fs}}$.

The block diagram corresponding to system (23) is shown in Fig. 2. Note that it contains the time derivatives of $\delta\omega$, δa_f and δb_f.

State-space expression of the linearized CFP models

Several analytical control design methods (like linear quadratic regulators, LQRs) are based on the state-space modelling. Linearized models (22) and (23) can be easily put into the state-space representation. Accordingly, the state-space representation associated with Q control structure is expressed in Eq. (24):

$$\begin{aligned} \frac{dX}{dt} &= A_Q \cdot X + B \cdot u + F_Q \cdot Z \\ y &= C \cdot X + D \cdot u \end{aligned} \tag{24}$$

where $X = [\ \delta Q \quad \delta\omega \quad \delta T\ ]^T, u = \delta f, Z = [\ \delta a_n \quad \delta a_f \quad \delta b_f \quad \delta\eta_f\ ]^T, A_Q = \begin{bmatrix} \frac{-k_{Qs}}{\chi_s} & \frac{k_{\omega s}}{\chi_s} & 0 \\ \frac{-k_{TQs}}{J_s} & \frac{-k_{T\omega Qs}}{J_s} & \frac{1}{J_s} \\ 0 & \frac{-\beta_s}{T_{es}} & \frac{-1}{T_{es}} \end{bmatrix}$,

$B = \begin{bmatrix} 0 \\ 0 \\ \frac{k_{fs}}{T_{es}} \end{bmatrix}$, $F_Q = \begin{bmatrix} \frac{-Q_s^2}{\chi_s} & \frac{-Q_s^2}{\chi_s} & \frac{-Q_s}{\chi_s} & 0 \\ 0 & \frac{k_{TafQs}}{J_s} & \frac{k_{TbfQs}}{J_s} & \frac{k_{T\eta s}}{J_s} \\ 0 & 0 & 0 & 0 \end{bmatrix}$, $C = [\ 1 \quad 0 \quad 0\ ]$ and $D = 0$.

The state-space model adopted for H control design is shown below.

$$\begin{aligned} \frac{dX}{dt} &= A_H.X + B.u + F_H.Z \\ y &= C.X + D.u \end{aligned} \tag{25}$$

where $X = [\ \delta H \quad \delta\omega \quad \delta T\ ]^T, u = \delta f, Z = [\ \delta a_n \quad \delta a_f \quad \delta b_f \quad \delta\eta\ ]^T$,

$A_H = \begin{bmatrix} \frac{-\left(k_{Hs}+k_{THs}.\frac{k_{H\omega ds}}{J_s}\right)}{\chi_s} & \frac{-\left(k_{H\omega s}+k_{T\omega Hs}.\frac{k_{H\omega ds}}{J_s}\right)}{\chi_s} & \frac{k_{H\omega ds}}{\chi_s} \\ \frac{-k_{THs}}{J_s} & \frac{-k_{T\omega Hs}}{J_s} & \frac{1}{J_s} \\ 0 & \frac{-\beta_s}{T_{es}} & \frac{-1}{T_{es}} \end{bmatrix}$, $B = \begin{bmatrix} 0 \\ 0 \\ \frac{k_{fs}}{T_{es}} \end{bmatrix}$,

$F_H = \begin{bmatrix} \frac{-Q_s^2}{\chi_s} & \frac{-\left(k_{Hafs}-k_{TafHs}.\frac{k_{H\omega ds}}{J_s}+k_{Hafds}.\frac{d}{dt}\right)}{\chi_s} & \frac{-\left(k_{Hbfs}-k_{TbfHs}.\frac{k_{H\omega ds}}{J_s}+k_{Hbfds}.\frac{d}{dt}\right)}{\chi_s} & \frac{k_{T\eta s}.\frac{k_{H\omega ds}}{J_s}}{\chi_s} \\ 0 & \frac{k_{TafHs}}{J_s} & \frac{k_{TbfHs}}{J_s} & \frac{k_{T\eta s}}{J_s} \\ 0 & 0 & 0 & 0 \end{bmatrix}$.

$C = [\ 1 \quad 0 \quad 0\ ], D = 0,$

Note that matrix F_H contains differentiation of disturbances. For both models (24) and (25), it is necessary to account for that usually the CFPs driven by induction motors are not equipped with the velocity and torque sensors. However, the estimates of the velocity and torque are available in real time through the monitoring systems of industrial variable speed AC drives feeding the motors. The linearization based on the Taylor expansion could also be applied for deriving these state-space linearized models. There are the same initial challenges: the six order of the nonlinear system, reducing the number of state variables via eliminating algebraic equations, and the model order reduction via simplifying assumptions. Compared to this method, the approach used in the paper avoids analytical differentiation procedure and does not require analytical approximation of polynomials for the combined efficiency.

Linearized model validation

Test rig description

The experimental setup was configured with a REM 48–0200-2D-07 industrial centrifugal fan manufactured by Nicotra-Gebhardt (refer to Figs. 3 and 4). The system operates optimally at a flow rate of 1215 m^3/h, a pressure of 680 Pa and the rotational speed of 2840 rpm, resulting in an overall efficiency of 53.5%. The fan is mechanically coupled to a 0.37 kW Siemens three-phase squirrel-cage induction motor (model 1LA9070-2KA11-Z) with a delta connection configuration. The nominal voltage is 230 V, the nominal stator phase current is 0.94 A, and the nominal velocity is the same as for the fan. Key electrical motor parameters were identified through standard no-load and rotor-lock testing procedures, yielding the following values: $R_s = 14.6\ \Omega$, $L_s = 1.1023$ H, $R_r = 16.53\ \Omega$, $L_r = 1.1023$ H and mutual inductance $L_m = 1.0541$ H. Therefore, for the rated operating conditions the drop of the voltage across the stator resistance is 5.9% of the rated voltage. Because of the fan's mechanical design, executing a traditional no-load test was not feasible without detaching the fan, as the fan assembly inherently imposes load torque on the motor. Additionally, secure rotor locking could not be achieved due to mechanical constraints. To mitigate alignment issues during disassembly and reassembly, a second motor, identical in specifications but not connected to the fan, was procured from the manufacturer and used exclusively for experimental characterization.

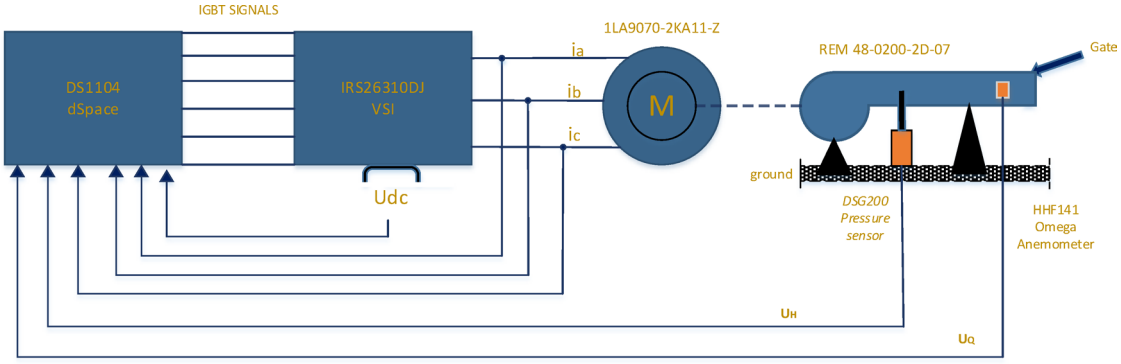


Fig. 3. Schematic representation of the hardware-in-the-loop (HIL) control prototyping setup for centrifugal fan units.

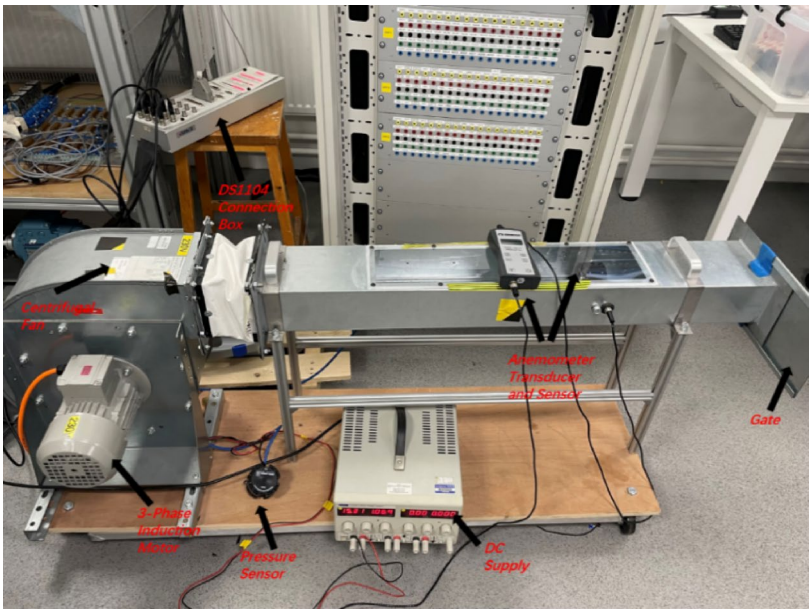


Fig. 4. The test rig of the centrifugal fan.

The IRS26310DJ gate driver evaluation board is employed to drive the induction machine via a 2-level, 3-phase full-bridge voltage-source-inverter (VSI) constructed using insulated-gate bipolar transistors (IGBTs). This system also features a single-phase full-bridge diode rectifier and a DC-link capacitor. The input voltage to the rectifier is 230 V RMS, and the inverter is rated for a continuous output power of 400W. The digital control functionality of the gate driver board is deactivated. A dSPACE DS1104 controller is used to implement key control functions including the generation of a ramp signal for frequency reference adjustment, V/f or V/f^2-based control algorithms, and sinusoidal pulse-width modulation (PWM). The controller also manages the analogue-to-digital conversion of DC-link voltage measurements, captured via an LV 25-P voltage sensor and stator current feedback, monitored using LTS 6-NP current sensors. PWM signals are transmitted to the gate driver board through digital isolators.

The outlet of the fan is connected to an air duct equipped with a manually adjustable gate, enabling control of the duct's cross-sectional area from fully open to completely closed positions. Airflow rate measurements are conducted using an Omega HHF141 anemometer, featuring an integrated turbine positioned within the duct. Pressure variations within the duct are captured by a Ziehl Abegg DSG2000 differential pressure sensor. Both sensors produce DC voltage outputs, which are digitized using the DS1104 data acquisition system. Additionally, an A2108 optical tachoprobe sensor is employed for recording rotational speed. All experimental measurements are logged via the dSPACE ControlDesk software.

Features of the simulations

The nonlinear centrifugal fan model was simulated using *MATLAB/Simulink/Simscape*. The induction motor was modeled through the *Induction Motor SI Units Block* from the *Specialized Power Systems toolbox*, configured in the stationary reference frame. A three-phase controlled voltage source provided V/f=constant control and a linearly increasing frequency input. The fan subsystem Eqs. (1)–(5) were implemented within Simulink. The experimentally identified parameters for the fan model are as follows[8]: H_{or}=1079 Pa, b_f=2039 Pa/(m^3/s), a_f =−1711 Pa/(m^3/s)^2, J=0.17 kg·m^2 and χ=5000 Pa·s/(m^3/s).

The combined efficiency estimator, defined as $\eta_c = f(Q, H, f)$, is implemented using a feedforward backpropagation ANN architecture. The network consists of three layers, containing 5, 5, 1 neurons, respectively. Hyperbolic tangent sigmoid (tansig) functions are used as activation functions in the first and second layers, while the output layer employs a linear (purelin) function. The ANN was developed and trained in MATLAB using the nnstart toolbox, based on 132 experimental steady-state data points. These data correspond to eleven fan performance curves collected at frequencies ranging from 30 to 50 Hz, in 2 Hz increments, as illustrated in Fig. 5a. For each frequency, Q and H were measured at twelve duct gate positions spaced at 1 cm intervals between 0 cm (fully open) and 11 cm (fully closed). The motor input active power, P_{in}, was calculated from the measured stator currents and the reference voltages, considering that the actual voltages are PWM. Consequently, the efficiency is computed using $\eta_c = QH/P_{in}$, as shown in Fig. 5b. The maximum relative error between the estimated and measured efficiency values was found to be 1.5%. In the nonlinear model simulations, motor efficiency (η_m) is calculated as the ratio of the difference between the motor's input active power and copper losses to the input active power. Other motor losses are reasonably attributed to the fan, as the resulting error in Q and H calculations remains below 5%, complying with the ISO 13348 standard. For the linearized model simulations, initial steady-state conditions, also required for determining model parameters, are derived from the nonlinear model. The independent variables include the supply frequency (f) and the parameter a_n, which is

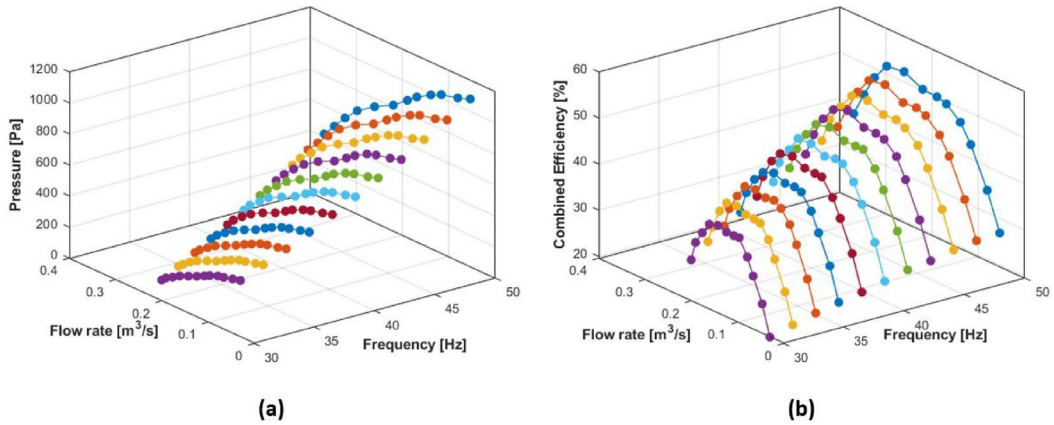


Fig. 5. Data representation of (**a**) $f - Q - H$ and (**b**) $f - Q - \eta_c$.

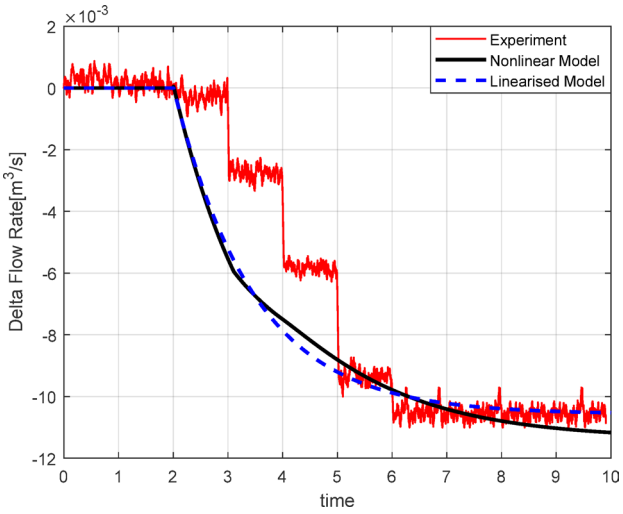


Fig. 6. Transient response of the flow rate deviation.

uniquely determined by the duct gate position. The results obtained from the block diagrams and corresponding state-space representations were verified to be identical.

Comparison between simulations and experimental data

Figures 6–8 illustrate the transient deviations caused by a 2 Hz step reduction in frequency (from 50 to 48 Hz, without ramping) at a duct gate opening of 7 cm, corresponding to a_n= 10,936 Pa/(m^3/s)^2. The associated steady-state conditions are Q_s=0.261 m^3/s, H_s=745 Pa and ω_s=308 rad/s. Experimental observations showed that the HHF141 Omega flow rate anemometer operates with a fixed sampling time, functioning similarly to a zero-order hold, as evident in Fig. 6. Likewise, the Ziehl Abegg DSG2000 differential pressure sensor incorporates sampling and filtering effects, as shown in Fig. 7. Since the fan's transient behavior evolves slowly, these sensors were adequate to capture the dynamics accurately. The results confirm a good agreement between the experimental data and both the nonlinear and linearized models, with accuracy conforming to ISO 13348 standards, and justify the assumption of neglecting the voltage drop across the stator resistance during the linearization. The parameterization of the nonlinear model is done for a specific operating point[8]. Since further the parameters are considered constant then the nonlinear model has different accuracy for different operating points, and this may favour the linearized model in accuracy for some instances like in Fig. 8.

The state-space descriptions (24) and (25) yield the following transfer functions:

$$W_Q(s) = \frac{\delta Q(s)}{\delta f(s)} = \frac{k_Q}{(T_\mu s + 1)(T_F^2 s^2 + 2\xi T_F s + 1)} \tag{26}$$

$$W_H(s) = \frac{\delta H(s)}{\delta f(s)} = \frac{k_H(T_H s + 1)}{(T_\mu s + 1)(T_F^2 s^2 + 2\xi T_F s + 1)} \tag{27}$$

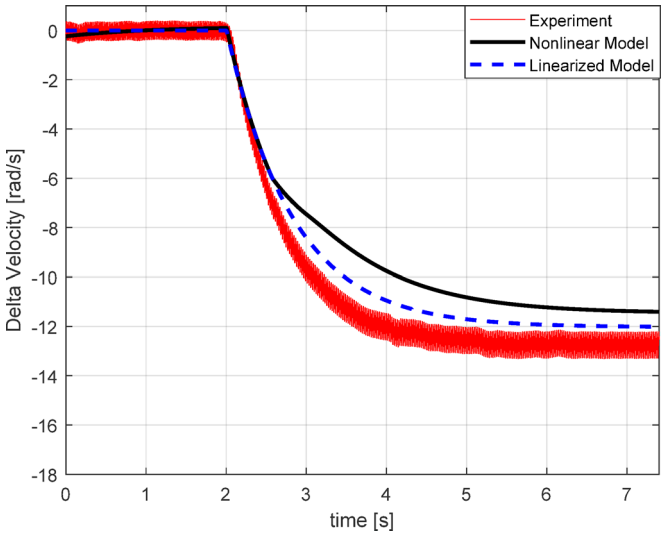


Fig. 8. Transient response of the velocity deviation.

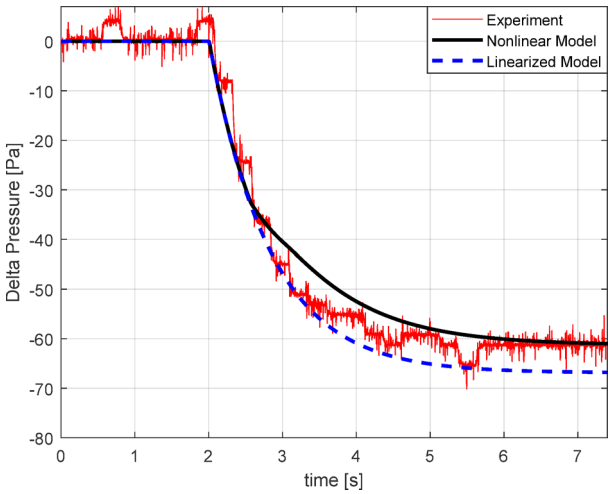


Fig. 7. Transient response of the pressure deviation.

where, for the specific conditions of Figs. 6 and 7, k_Q= 0.0065 m^3/(s·Hz), k_H= 37.18980 Pa/Hz, T_μ= 0.00570 s, T_H= 0.8757 s, T_F = 0.7706 s and ξ= 0.9945.

The transfer function which relates the velocity deviation and the frequency perturbation can be obtained either from (24) or from (25) with $\boldsymbol{C} = [\ 0 \quad 1 \quad 0\ ]$.

$$W_\omega(s) = \frac{\delta\omega(s)}{\delta f(s)} = \frac{k_\omega(T_\omega s + 1)}{(T_\mu s + 1)(T_F^2 s^2 + 2\xi T_F s + 1)} \tag{28}$$

where k_ω= 5.9416 rad/(s·Hz) and T_ω= 0.7294 s for the case of Fig. 8. Note that $T_H s + 1$ in the numerator of $W_H(s)$ and $T_\omega s + 1$ in the numerator of $W_\omega(s)$ cause the faster initial rate of change of δH and $\delta\omega$ compared to δQ. Since T_H and T_ω are close then the velocity and pressure deviations change almost synchronously. The results remained similar for multiple initial operating points under small frequency step variations.

Assuming that χ is a small value approaches the dynamical fan model to quasi-steady one. For χ=0.1 Pa·s/(m^3/s) and the steady-state conditions in Figs. 6–8, the transfer functions are as follows

$$W_Q(s) = \frac{k_Q}{(T_\mu s + 1)(T_\nu s + 1)(T_{F1} s + 1)} \approx \frac{k_Q}{(T_\mu s + 1)(T_{F1} s + 1)} \tag{29}$$

$$W_H(s) = \frac{k_H(T_{H1} s + 1)}{(T_\mu s + 1)(T_\nu s + 1)(T_{F1} s + 1)} \approx \frac{k_H}{(T_\mu s + 1)(T_{F1} s + 1)} \tag{30}$$

$$W_\omega(s) = \frac{k_\omega\,(T_{\omega 1}s+1)}{(T_\mu s+1)\,(T_\nu s+1)\,(T_{F1}s+1)} \approx \frac{k_\omega}{(T_\mu s+1)\,(T_{F1}s+1)} \tag{31}$$

where T_{F1}= 0.8143 s and T_ν= 0.0000146 s, T_{H1}= 0.0000175 s, $T_{\omega 1}$= 0.0000146 s are negligible time constants. This means that both δQ and δH change synchronously with the change of $\delta\omega$ which contradicts the experiments[8] ignoring the δQ transients in the fan housing.

Possible control design options

Although control design and its evaluation are beyond the scope of the paper, this section briefly discusses possibility of using the developed linearized models for the control design based on classic and modern design methodologies, convenient for practical engineers, instead of heuristic solutions. The open-loop transfer functions for Q and H given in Eq. (26) and (27) allow simple application of the Modulus Optimum tuning method[30] yielding fast aperiodic responses characterized by a 4.3% maximum overshoot and a transient time of 11 T_μ, where T_μ represent a small time constant. To obtain Modulus Optimum, the open-loop target transfer function is chosen as:

$$W_{des}(s) = \frac{1}{2T_\mu s\,(T_\mu s+1)} \tag{32}$$

This leads to the formation of a PID Q controller:

$$W_{QC}\,(s) = \frac{W_{des}\,(s)}{W_Q\,(s)} = k_{pQ}\frac{T_dT_is^2+T_is+1}{T_is}, \tag{33}$$

and a PID H controller with an aperiodic filter

$$W_{HC}\,(s) = \frac{W_{des}\,(s)}{W_H\,(s)} = k_{pH}\frac{T_dT_is^2+T_is+1}{T_is}\frac{1}{T_H+1}, \tag{34}$$

where $k_{pQ} = \frac{\xi T_F}{T_\mu k_Q}, T_i = 2\xi T_F, T_d = \frac{T_F}{2\xi}, k_{pH} = \frac{\xi T_F}{T_\mu k_H}$.

The methodology is convenient for the control implementation based on industrial AC drives which already contain embedded PID controllers, provide access to their parameterization and feedback voltage connection (only Q or H measurement or estimation is required).

The state-space representations (24) and (25) can directly be used for LQR design. However, to provide zero flow rate and pressure steady-state errors the models must be augmented with additional state coordinates as integrals of Q and H dynamical errors, respectively, and corresponding equations[31].

$$\frac{d\delta Q_{in}}{dt} = \delta Q - \delta Q^*,\ X = \begin{bmatrix}\ \delta Q_{in} & \delta Q & \delta\omega & \delta T\ \end{bmatrix}^T \tag{35}$$

$$\frac{d\delta H_{in}}{dt} = \delta H - \delta H^*,\ X = \begin{bmatrix}\ \delta H_{in} & \delta H & \delta\omega & \delta T\ \end{bmatrix}^T \tag{36}$$

where '*' denotes corresponding reference values, and for stabilization systems $\delta Q^* = 0$ and $\delta H^* = 0$.

The following cost function is to be minimized for each system

$$\min_u J = \int_0^\infty \left(\sum_{i=1}^4 \alpha_i x_i^2 + cu^2\right) dt, \tag{37}$$

where α_i and c are positive weighting constants. The required analytical derivations of the LQR controllers given in (38) can be replaced by numerical computations of the feedback gains k_i using lqr command in Matlab.

$$u = -\sum_{i=1}^4 k_i x_i \tag{38}$$

The technical implementation requires measurements or real-time estimation of Q (or H), ω and T. It is more challenging for industrial applications than MO technique (an external microcontroller must be added to the AC industrial drive).

The transfer functions (26) and (27) can also be used to design the robust H_∞ controllers with mixed sensitivity loops shaping[32]. The procedure of the H_∞ controllers synthesis is applied to the weighted control system as the augmented controlled plant.

$$\begin{bmatrix} z \\ e \end{bmatrix} = \begin{bmatrix} P_{11} & P_{12} \\ P_{21} & P_{22} \end{bmatrix} \begin{bmatrix} w \\ u \end{bmatrix} \tag{39}$$

where w is the reference ($w = \delta Q^*$ for the flow rate control or $w = \delta H^*$ for H control), $u = \delta f$ is the control input, $z = \begin{bmatrix}\ z_1 & z_2 & z_3\ \end{bmatrix}^T$ are the error outputs, $e = w - y$ is the controller input ($y = \delta Q$ or

$y = \delta H$), $P_{11} = \begin{bmatrix} W_1 & 0 & 0 \end{bmatrix}^T$, $P_{12} = \begin{bmatrix} -W_1 G & W_2 & W_3 G \end{bmatrix}^T$, $P_{21} = 1$, $P_{22} = -G$, $G = W_Q(s)$ or $G = W_H(s)$, $W_i(s)$ is the weighting function for z_i. Then, the closed-loop transfer function from w to z is

$$M(s) = \begin{bmatrix} W_1 S & W_2 K S & W_3 T \end{bmatrix}^T \tag{40}$$

where K is the transfer function of the controller, $S = (1 + GK)^{-1}$ is the sensitivity function, $T = 1 - S$ is the complementary sensitivity function.

The design procedure seeks the controller K that minimizes $\|M(s)\|_\infty$ (the largest singular value across frequencies) to keep z small, and the analytical derivations can be replaced by a numerical solution using mixsyn Matlab command. It is achieved with the constraint $\|M(s)\|_\infty \leq 1$, ($\|S\|_\infty \leq \left|W_1^{-1}\right|$, $\|KS\|_\infty \leq \left|W_2^{-1}\right|$ and $\|T\|_\infty \leq \left|W_3^{-1}\right|$) to be applied for the selection of the weighting functions. Without restricting the control effort, W_2 is omitted:$M(s) = \begin{bmatrix} W_1 S & W_3 T \end{bmatrix}^T$. W_1 and W_3 are chosen as low-pass and high-pass filters[32], respectively, to provide good reference tracking and disturbance rejection performance, and robustness and noise attenuation. The designed Q and H controllers are of fifth order. They compensate all poles and zeros of the corresponding open loop transfer function G and reshape the loop according to the optimisation procedure. The software of the industrial AC drives needs to be updated by the manufacturers to implement the designed controllers instead of the imbedded PID controller available for parameterization (or an external microcontroller can be used).

The designed controllers should be tested via simulations of their operation within the nonlinear model preceding technical implementation and if necessary, controllers' parameters can be adjusted to provide satisfactory control quality. The linearization is done around an arbitrary operating point, so the controllers' parameters can be obtained for various operating points and updated accordingly. Alternatively, robust adaptive controllers can be designed[33].

Conclusion

The paper derives a reduced-order control-oriented linearized model of the FP powered by an induction machine based on its dynamical nonlinear model. Due to complexity and nonlinearity of the combined system (both the FP model itself and the motor model are nonlinear), the linearization procedure is not straightforward. The objective is reached through rearranging the FP model itself and using a specific reference frame for the motor modelling aligned with the stator voltage vector. The linearized model is validated via a step response simulation compared with the combined nonlinear model and with experimental data. The model relates small deviations of the stator voltage frequency to corresponding small deviations of Q and H, suitable for scalar induction motor regulation applications. It is presented in state-space forms, as block diagrams and as transfer functions suitable for systematic closed-loop control design of Q and H. The linearized model is convenient for practical engineers in the area of automation of air and water supply systems via AC drives applications.

Data availability

The datasets used and/or analysed during the current study available from the corresponding author on reasonable request.

Received: 28 August 2025; Accepted: 5 November 2025
Published online: 29 November 2025

References

1. Turkeri, C. & Kiselychnyk, O. Improved flow rate and pressure ANN estimators for a centrifugal fan with induction motor drive. *J. Energy Syst.* **8**(3), 130–142. https://doi.org/10.30521/jes.1254552 (2024).
2. Arribas, J. & González, C. Optimal vector control of pumping and ventilation induction motor drives. *IEEE Trans. Ind. Electron.* **49**, 889–895. https://doi.org/10.1109/TIE.2002.801240 (2002).
3. Giannoutsos, S. V. & Manias, S. N. A data-driven process controller for energy-efficient variable-speed pump operation in the central cooling water system of marine vessels. *IEEE Trans. Ind. Electron.* **62**(1), 587–598. https://doi.org/10.1109/TIE.2014.2317456 (2015).
4. Corgnati, S., Orlietti, L., Mitolo, M. & Tartaglia, M. Energy savings in integrated urban water systems: A case study, in *2017 IEEE/IAS 53rd Industrial and Commercial Power Systems Technical Conference (I&CPS)*, Niagara Falls, ON, Canada, 1–4 (2017). https://doi.org/10.1109/ICPS.2017.7945090.
5. Eto, J. H. & de Almeida, A. Saving electricity in commercial buildings with adjustable-speed drives. *IEEE Trans. Ind. Appl.* **24**(3), 439–443. https://doi.org/10.1109/28.2893 (1988).
6. Gevorkov, L., Rassõlkin, A., Kallaste, A. & Vaimann, T. Simulink-based model for flow control of a centrifugal pumping system, in *Proceedings of 25th International Workshop Electric Drives (IWED)*, Moscow, Russia, 1–4 (2018). https://doi.org/10.1109/IWED.2018.8321399.
7. Gevorkov, L., Vodovozov, V. & Raud, Z. Simulation study of the pressure control system for a centrifugal pump, in *Proceedings of RTUCON*, Riga, Latvia, 1–5 (2016). https://doi.org/10.1109/RTUCON.2016.7763086.
8. Turkeri, C. & Kiselychnyk, O. Dynamical modelling of a centrifugal fan driven by an induction motor and experimental validation. *Energies* **16**(18), 6658. https://doi.org/10.3390/en16186658 (2023).
9. Schneider Electric, *Altivar Machine ATV320 Variable Speed Drives for Asynchronous and Synchronous Motors Installation Manual*, Document No. NVE41289, Version 09, April 2025. [Online]. Available: https://www.se.com/us/en/download/document/NVE41289/
10. ABB, *ACS550-01/U1 User's Manual* (0.75…160 kW / 1…200 hp), Rev. H, 2014. [Online]. Available https://library.e.abb.com/public/313b6ebaf237059fc1257d0a0048fd68/EN_ACS550_01_UM_H_A4.pdf.
11. Travieso-Torres, J. C., Contreras-Jara, C., Diaz, M., Aguila-Camacho, N. & Duarte-Mermoud, M. A. New adaptive starting scalar control scheme for induction motor variable speed drives. *IEEE Trans. Energy Convers.* **37**(1), 729–736. https://doi.org/10.1109/TEC.2021.3108664 (2022).

12. Kiselychnyk, O. I. & Bodson, M. Nonsensor control of centrifugal water pump with asynchronous electric-drive motor based on extended Kalman filter. *Russ. Electr. Eng.* **82**(2), 69–75. https://doi.org/10.3103/S1068371211020088 (2011).
13. Kallesoe, C. S., Cocquempot, V. & Izadi-Zamanabadi, R. Model based fault detection in a centrifugal pump application. *IEEE Trans. Control Syst. Technol.* **14**(2), 204–215. https://doi.org/10.1109/TCST.2005.860524 (2006).
14. Murshid, S. & Singh, B. Double-stage solar PV array fed water pump driven by permanent magnet synchronous motor. *IEEE Trans. Ind. Appl.* **57**(2), 1736–1745. https://doi.org/10.1109/TIA.2020.3046457 (2021).
15. Kolhe, M., Joshi, J. C. & Kothari, D. P. Performance analysis of a directly coupled photovoltaic water-pumping system. *IEEE Trans. Energy Convers.* **19**(3), 613–618. https://doi.org/10.1109/TEC.2004.827032 (2004).
16. Weigand, H. & Eddy, L. B. Centrifugal pump and compressor characteristics. *Electr. Eng.* **79**, 576–582. https://doi.org/10.1109/EE.1960.6432712 (1960).
17. Emami, S. A. & Emami, M. H. Design and implementation of an online precise monitoring and performance analysis system for centrifugal pumps. *IEEE Trans. Ind. Electron.* **65**(2), 1636–1644. https://doi.org/10.1109/TIE.2017.2723875 (2018).
18. Pottebaum, J. R. Optimal characteristics of a variable-frequency centrifugal pump motor drive. *IEEE Trans. Ind. Appl.* **I-A20**(1), 23–31. https://doi.org/10.1109/TIA.1984.4504371 (1984).
19. Omar, A. K., Khaldi, A. & Ladouani, A. Prediction of centrifugal pump performance using energy loss analysis. *Aust. J. Mech. Eng.* **15**, 210–221. https://doi.org/10.1080/14484846.2016.1252567 (2017).
20. Barbarelli, S., Amelio, M. & Florio, G. Predictive model estimating the performances of centrifugal pumps used as turbines. *Energy* **107**, 103–121. https://doi.org/10.1016/j.energy.2016.03.122 (2016).
21. Ahonen, T. et al. Estimation of pump operational state with model-based methods. *Energy Convers. Manag.* **51**(6), 1319–1325. https://doi.org/10.1016/j.enconman.2010.01.009 (2010).
22. Janevska, G. Mathematical modeling of pump system, in *Proceedings of 2nd Electronic International Interdisciplinary Conference*, Zilina, Slovakia, Sep. 2–6, 455–458 (2013).
23. Ahonen, T. et al. Frequency-converter-based hybrid estimation method for the centrifugal pump operational state. *IEEE Trans. Ind. Electron.* **59**(12), 4803–4809. https://doi.org/10.1109/TIE.2011.2176692 (2012).
24. Tamminen, J. et al. Comparison of model-based flow rate estimation methods in frequency-converter-driven pumps and fans. *Energy Effic.* **7**(3), 493–505. https://doi.org/10.1007/s12053-013-9234-6 (2014).
25. Wu, Q., Shen, Q., Wang, X. & Yang, Y. Estimation of centrifugal pump operational state with dual neural network architecture based model. *Neurocomputing* **216**, 102–108. https://doi.org/10.1016/j.neucom.2016.07.035 (2016).
26. Turkeri, C. & Kiselychnyk, O. Dynamical flow rate and pressure artificial neural network estimators for a centrifugal fan driven by an induction motor drive, in *Proceedings of IEEE ONCON*, Kharagpur, India, 1–6 (2022). https://doi.org/10.1109/ONCON56984.2022.10126880.
27. Burian, S. O. et al. Energy-efficient control of pump units based on neural-network parameter observer. *Tech. Electrodyn.* https://doi.org/10.15407/techned2020.01.071 (2020).
28. Pechenik, M. et al. Sensorless control of water supply pump based on neural network estimation. *Electrotech. Comput. Syst.* **3**(79), 462–466 (2015).
29. Krause, P. C., Wasynczuk, O. & Sudhoff, S. D. *Analysis of Electric Machinery and Drive Systems*. Wiley-IEEE Press (2002). https://doi.org/10.1002/9781118524336.
30. Suul, J. A., Molinas, M., Norum, L. & Undeland, T. Tuning of control loops for grid connected voltage source converters, in *2008 IEEE 2nd International Power and Energy Conference*, Johor Bahru, Malaysia, 797–802 (2008). https://doi.org/10.1109/PECON.2008.4762584.
31. Liu, H., Wang, J. & Kiselychnyk, O. Mathematical modeling and control of a cost effective AC voltage stabilizer. *IEEE Trans. Power Electron.* **31**(11), 8007–8016. https://doi.org/10.1109/TPEL.2015.2514180 (2016).
32. Dey, N., Mondal, U. & Mondal, D. Design of a H-infinity robust controller for a DC servo motor system, in *2016 International Conference on Intelligent Control Power and Instrumentation (ICICPI)*, Kolkata, India, 27–31 (2016). https://doi.org/10.1109/ICICPI.2016.7859667.
33. Mercorelli, P. Robust adaptive soft landing control of an electromagnetic valve actuator for camless engines. *Asian J. Control* **18**(4), 1299–1312. https://doi.org/10.1002/asjc.1250 (2016).

Author contributions

Cebrail Turkeri, Oleh Kiselychnyk: Conceptualization, Methodology, Software, Visualization, Investigation, Writing- Original draft preparation, Serdar Ekinci, Davut Izci: Data curation, Validation, Supervision, Resources, Writing—Review & Editing. Mohit Bajaj, Oleksandr Rubanenko: Project administration, Supervision, Resources, Writing—Review & Editing.

Funding

This research received no specific grant from any funding agency in the public, commercial, or not-for-profit sectors.

Declarations

Competing interests

The authors declare no competing interests.

Additional information

Correspondence and requests for materials should be addressed to M.B. or O.R.

Reprints and permissions information is available at www.nature.com/reprints.

Publisher's note Springer Nature remains neutral with regard to jurisdictional claims in published maps and institutional affiliations.

Open Access This article is licensed under a Creative Commons Attribution-NonCommercial-NoDerivatives 4.0 International License, which permits any non-commercial use, sharing, distribution and reproduction in any medium or format, as long as you give appropriate credit to the original author(s) and the source, provide a link to the Creative Commons licence, and indicate if you modified the licensed material. You do not have permission under this licence to share adapted material derived from this article or parts of it. The images or other third party material in this article are included in the article's Creative Commons licence, unless indicated otherwise in a credit line to the material. If material is not included in the article's Creative Commons licence and your intended use is not permitted by statutory regulation or exceeds the permitted use, you will need to obtain permission directly from the copyright holder. To view a copy of this licence, visit http://creativecommons.org/licenses/by-nc-nd/4.0/.

© The Author(s) 2025